Supporting Information

Boosting excitons dissociation in anion and cation co-doped polymeric semiconductor for selective oxidation reaction

Junkang Ge, Jun Zhao, Lei Li, Zhihao Li, Hui Wang*, Xiaodong Zhang*, and Yi Xie

Hefei National Research Center for Physical Sciences at the Microscale, University of Science and Technology of China, Hefei, 230026, P. R. China.

Experimental section:

Materials. Thiourea, potassium chloride (KCl), sodium bicarbonate ($NaHCO_3$), potassium bicarbonate ($KHCO_3$), ammonium chloride (NH_4Cl), ammonium bromide (NH_4Br), ammonium iodide (NH_4I), acetonitrile (CH_3CN, AR), methanol (MeOH, AR), and anhydrous ethanol (EtOH, AR) were purchased from Sinopharm Chemical Reagent Co., Ltd. Nitrotetrazolium Blue chloride (NBT), 5,5-dimethyl-1-pyrroline N-oxide (DMPO, for ESR tests) and phenylboronic acid were purchased from Energy-Chemical. The water used in the work was deionized (DI) water. All reagents were used directly without further purification.

Preparation of polymeric carbon nitride (PCN). The PCN was obtained through the polymerization of thiourea under high temperatures. In a typical synthesis procedure, 10 g of thiourea were placed into a crucible (30 mL) with a cover and then heated at 550℃ for 2 hours in a muffle furnace with a heating rate of approximately 5℃/min. After the thermal treatment, the crucible was cooled to room temperature in the muffle furnace. The yellow product obtained was collected and thoroughly ground, resulting in the powder samples referred to as PCN.

Preparation of K^+, Cl^- co-doped polymeric carbon nitride (KCl-CN). The KCl-CN was synthesized by polymerizing thiourea with K ion source, and Cl ion source under high temperatures. In detail, 10 g of thiourea and a predetermined amount of potassium chloride (or potassium bicarbonate ($KHCO_3$) and ammonium chloride (NH_4Cl) instead), were dissolved in 30 mL of distilled water. The solution was heated to 80°C for 12 hours to obtain the solid precursor. Then, the solid precursor was placed into a crucible (30 mL) with a cover and heated at 550°C for 2 hours in a muffle furnace with a heating rate of approximately 5°C/min. After the thermal treatment, the crucible was cooled to room temperature in the muffle furnace. The solid product was collected by centrifugation, washed three times with deionized water and ethanol, and then dried at 60°C for 12 hours under vacuum. The obtained yellow product with 3% content of added salt was defined as KCl-CN. In addition, we adopted the same synthesis method, using potassium bicarbonate and ammonium chloride as sources of K^+ and Cl^- to synthesize individual ion doped samples of K-CN and Cl-CN.

Preparation of other anion (Cl^-, Br^-, I^-) and cation (Na^+, K^+) co-doped samples. These samples were prepared by similar method as that of KCl-CN with the change of anion and cation sources. In detail, the Cl^-, Br^-, I^- source were ammonium chloride (NH_4Cl), ammonium bromide (NH_4Br) and ammonium iodide (NH_4I), and the Na^+, K^+ sources were sodium bicarbonate ($NaHCO_3$) and potassium bicarbonate ($KHCO_3$). The as-prepared samples are defined as, NaCl-CN, NaBr-CN, NaI-CN, KBr-CN and KI-CN, respectively.

Nitrotetrazolium Blue chloride reaction Measurements. In detail, 20 mg of catalyst was added to a 50 mL solution of NBT in water, with a concentration of 15 mg/L. The solution was stirred in the dark for 30 minutes to achieve adsorption and desorption equilibrium. Then, the mixture was illuminated using a xenon lamp (Au-Light CEL-HXF300) with a 400 nm cut-off filter. The UV-vis spectra were measured at 5 minutes intervals by monitoring the absorbance in the range of 200 to 500 nm.

Measurements for Electron Spin Resonance Trapping. In detail, a 50 μL suspension of samples (5

g/L) was dispersed in a 500 μL methanol solution of 5,5-dimethyl-1-pyrroline-N-oxide (DMPO, 20 mM). After being illuminated for 1 minutes using a xenon lamp (Au-Light CEL-HXF300) with a 400 nm cut-off filter as the light source, the mixture was examined using a Bruker EMX plus model spectrometer operating at the X-band frequency (9.4 GHz) under room temperature.

Photocatalytic Selective Oxidation of phenylboronic acid Measurements. 10 mg of catalyst and 0.1 mmol of phenylboronic acid were added to a mixture of 1 mL of methanol and 1 mL of acetonitrile in a 10 mL quartz tube with a rotor. After sonicating for a few seconds, the mixed solution was bubbled with oxygen for 5 minutes. Afterwards, the sealed tube was irradiated by a xenon lamp (Au-Light CEL-HXF300) equipped with a 400 nm cut-off filter as the light source while vigorously stirring for 4 hours at 298 K. The resulting solution was then centrifuged and examined using ^{1}H NMR spectroscopy, with 1,1,2,2-tetrachloroethane used as the internal standard substance.

Electrochemical test. The electrochemical tests were performed in a conventional three-electrode cell containing a 0.5 M Na_2SO_4 solution with a -0.4 V bias relative to an Ag/AgCl electrode, using an electrochemical workstation (CHI760E, Shanghai Chenhua Limited, China). In detail, a cleaned indium tin oxide (ITO) substrate coated with the sample film served as the working electrode, a platinum (Pt) wire acted as the counter electrode and a standard Ag/AgCl electrode was used as the reference electrode. The sample electrode, with an area of approximately 1 cm^2, was prepared by depositing 100 μL of an aqueous slurry consisting of 30 mg of the prepared samples, 250 μL of ethanol, 750 μL of water and 100 μL of naphthol onto a cleaned indium tin oxide (ITO) glass substrate. The periodic on/off photocurrent response plots were recorded under ambient conditions and irradiated by a xenon lamp (Au-Light CEL-HXF300) equipped with a 400 nm cut-off filter. Mott-Schottky tests were performed with potentials ranging from -1 V to 1 V (vs. Ag/AgCl) at selected frequencies of 500, 800 and 1000 Hz. Electrochemical impedance spectroscopy (EIS) was performed over a frequency range of 0.01 Hz to 10^6 Hz with an AC voltage amplitude of 5 mV.

Calculation method. The present first principle DFT calculations are performed by Vienna Ab initio Simulation Package (VASP) with the projector augmented wave (PAW) method. The exchange-functional is treated using the generalized gradient approximation (GGA) of Perdew-Burke-Ernzerhof (PBE) functional. The energy cutoff for the plane wave basis expansion was set to 450 eV and the force on each atom less than 0.02 eV/Å was set for convergence criterion of geometry relaxation. The computational model was constructed by a 2×2 supercell of C_3N_4. 15 Å vacuum was added along the z direction to avoid the interaction between periodic structures. The Brillouin zone integration is performed using 3×3×1 k-point sampling. The self-consistent calculations apply a convergence energy threshold of 10^{-5} eV. The surface electrostatic potential calculations were employed by Gaussian 09 software, and B3LYP/6-311G method was used for molecular optimization.

Characterization Methods. The powder X-ray diffraction (PXRD) patterns were acquired using a Philips X'Pert Pro Super diffractometer with Cu Kα radiation (λ = 1.54178 Å). The scanning electron microscopy (SEM) images were recorded using a JEOL JSM-6700F SEM. The transmission electron microscopy (TEM) and the energy dispersive spectrometer (EDS) was recorded employing a JEM-2100F field-emission electron microscope at an acceleration voltage of 200 kV. The fourier transform infrared (FT-IR) spectra were obtained using a Magna-IR750 FT-IR spectrometer in a KBr pellet, scanning from

4000 to 400 cm^{-1} under room temperature. The ultraviolet–visible (UV–vis) spectra were recorded using a Perkin Elmer Lambda 950 UV–vis–NIR spectrophotometer. The nuclear magnetic resonance Spectroscopy (NMR) experiments were performed with a 400-MHz Bruker AVANCE AV III NMR spectrometer. The steady-state fluorescence (FL) and phosphorescence (PL) spectra as well as the time-resolved phosphorescence spectra were obtained using a FLUOROLOG-3-TAU fluorescence spectrometer equipped with an integrating sphere. The X-ray photoelectron spectra (XPS) were recorded on an ESCALAB MKII with Mg Kα as the exciltation source by referencing C 1s to 284.8 eV. The electron spin resonance (EPR) spectra were collected using a JEOL JES-FA200 electron spin resonance spectrometer (298 K, 9.062 GHz).

Supplementary figures and table

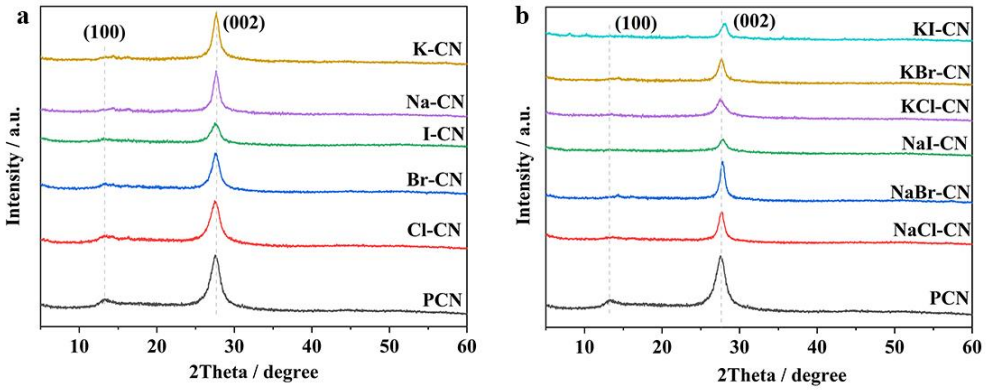

Figure S1. Powder XRD patterns of (a) individual ion doped samples of with cations of (Na^+, K^+), or anions of (Cl^-, Br^-, I^-); (b) different anions (Cl^-, Br^-, I^-) and cations (Na^+, K^+) co-doped polymeric carbon nitride. All samples were measured under the same conditions, and the pattern of PCN was taken as a reference with the same data in all the figures.

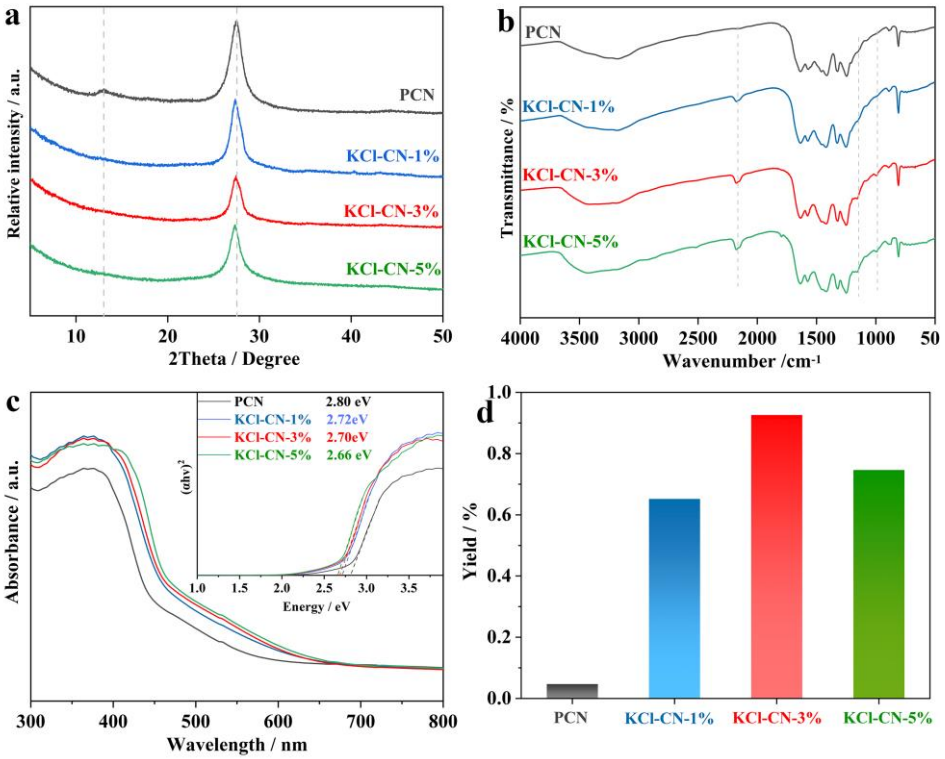

Figure S2. (a) Powder XRD pattern, (b) FT-IR spectra, (c) UV-vis spectra (Inset: corresponding Tauc plots) and (d) Oxidation yield of phenylboronic acid in samples with different doping amounts of K^+, Cl^-.

Herein, we have prepared a series of K^+, Cl^- co-doped PCN with varying K^+ and Cl^- content of 1%, 3% and 5% in mass ratio during the preparation experiments, which are referred to as KCl-CN-1%, KCl-CN-3% and KCl-CN-5% for control experiment. As shown in **Figure S2a**, the Powder X-ray diffraction (PXRD) patterns show the location of the (002) peak intensity gradually decreases with an increase amount of K^+ and Cl^-. It is demonstrated from the Fourier transform infrared spectra (FT-IR) that the peak appearing at 992, 1154 and 2181 cm^{-1} progressively get stronger with the increase in K^+, Cl^- content (**Figure S2b**). Ultraviolet-visible (UV-vis) spectra and the corresponding Tauc plots were shown in **Figure S2c**, where the band gap of PCN was gradually decreased with the increasing in K^+, Cl^- content. The photocatalytic activity of samples was evaluated by the photooxidation of phenylboronic acid into phenol (**Figure S2d**), where KCl-CN-3% exhibited the best performances among the samples.

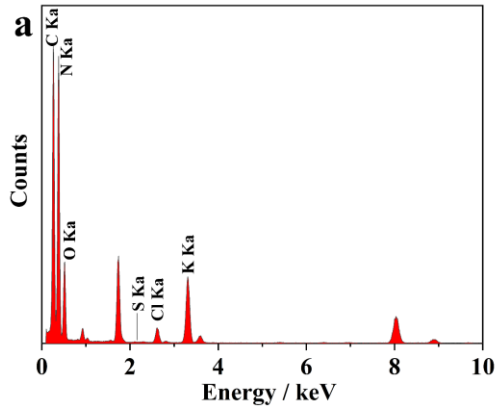

b

	Weight percentage / %	Atomic percent / %
C	49.6	57.6
N	32.34	32.16
O	7.34	6.39
K	8.8	3.13
Cl	1.77	0.69
S	trace	trace

Figure S3. (a) EDS spectrum of KCl-CN; (b) Element Content table of KCl-CN by EDS results.

As shown in Energy-Dispersive X-ray spectrum of KCl-CN (**Figure S3a** and **S3b**), the atomic percentage of the doped K^+ and Cl^- was determined to be 3.13% and 0.69%, respectively. Part of the Cl^- combines with the amino group during the thermal polymerization process to form ammonium chloride, resulting in the relatively low content of Cl ions.[1]

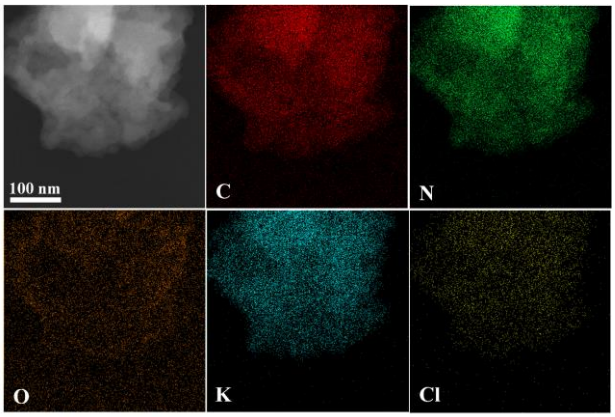

Figure S4. Energy dispersive spectrometer (EDS) elemental mapping results of KCl-CN.

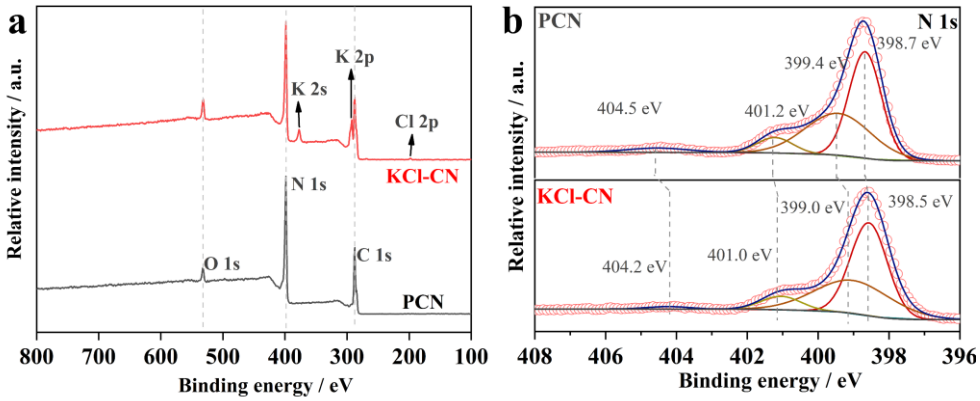

Figure S5. (a) XPS survey spectra and (b) N 1s spectra of PCN and KCl-CN.

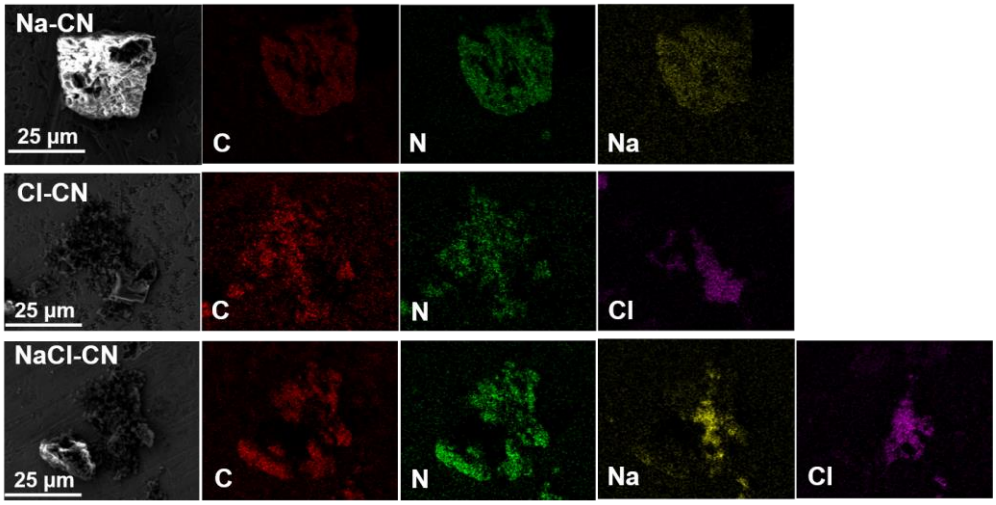

Figure S6. Elemental mapping by SEM-EDX analysis for Na-CN, Cl-CN and NaCl-CN.

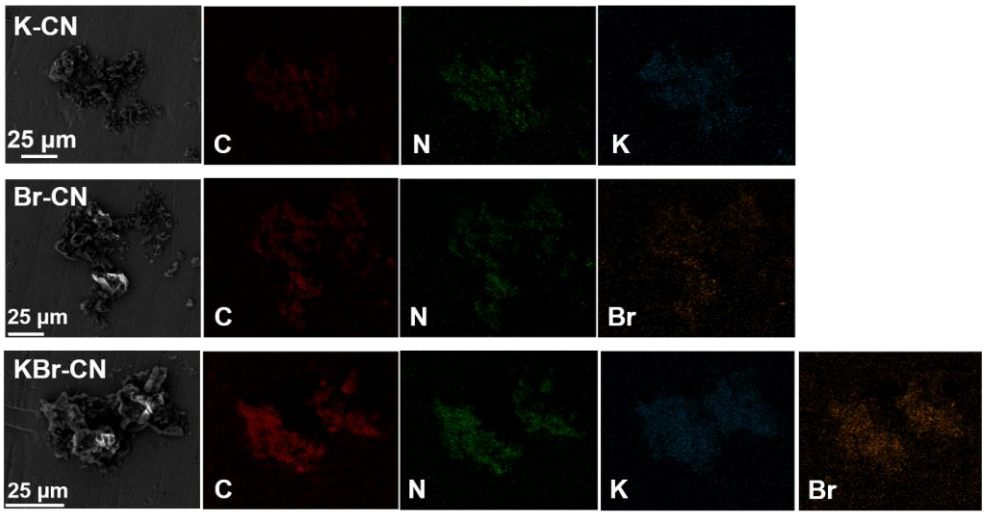

Figure S7. Elemental mapping by SEM-EDX analysis for K-CN, Br-CN and KBr-CN.

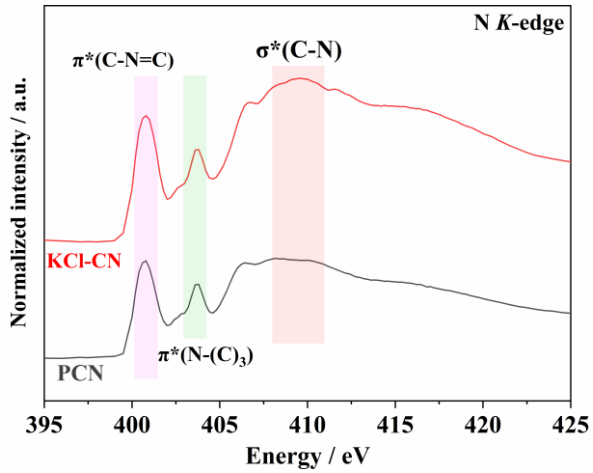

Figure S8. N *K*-edge XANES curves of PCN and KCl-CN.

The N *K*-edge synchrotron-based XANES spectra of PCN and KCl-CN observe absorption peaks appearing at 400.7 and 403.7 eV, which can be assigned to N in C=N-C and N-$(C)_3$ moieties, respectively. Nevertheless, KCl-CN displays a broad peak centered at 409.5 eV, corresponding to electron transition from the N 1s to C-N σ^* orbital.[2,3]

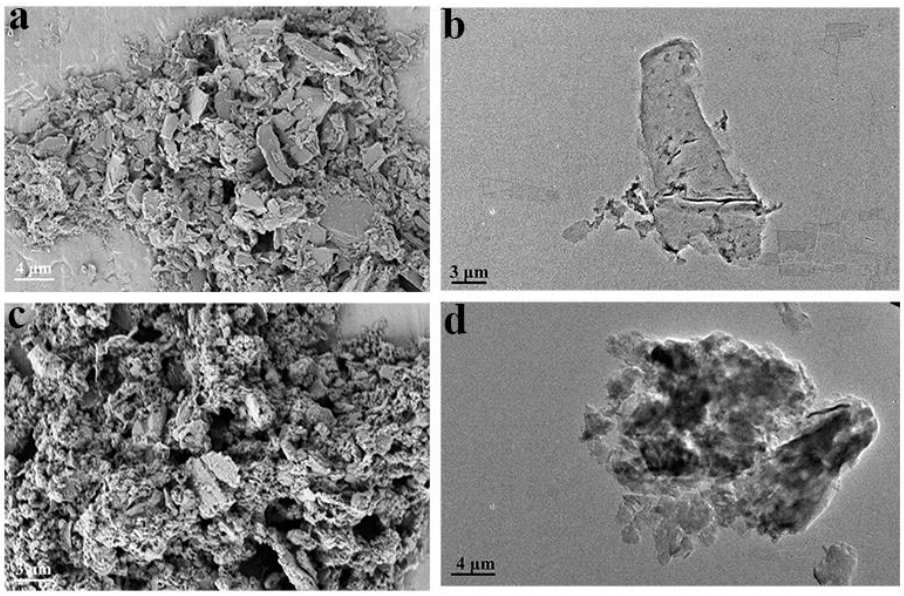

Figure S9. The scanning electron microscopy (SEM) and transmission electron microscopy (TEM) photographs of (a) (b) PCN and (c) (d) KCl-CN.

Both transmission electron microscopy (TEM) and scanning electron microscopy (SEM) are reliable methods for observing the morphology of materials. The morphology and structure (**Figure S9**) of KCl-CN exhibit smaller and thinner aggregated nanosheets than PCN, indicating that the incorporation of K^+ and Cl^- ions play an influence on the growth of PCN.

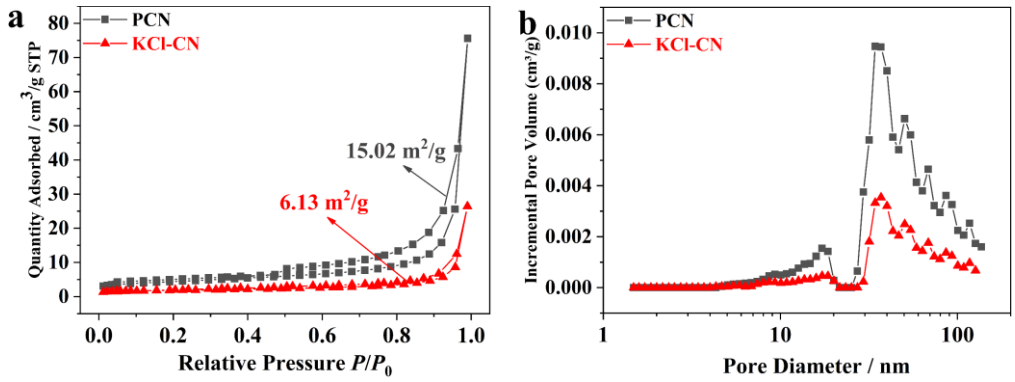

Figure S10. (a) Nitrogen adsorption-desorption isotherms and (b) pore size distribution spectra of PCN and KCl-CN.

As shown in **Figure S10**, the nitrogen adsorption-desorption isotherms exhibit KCl-CN possesses a smaller specific surface area and the same pore size distribution as PCN, which is consistent with the SEM and TEM results.

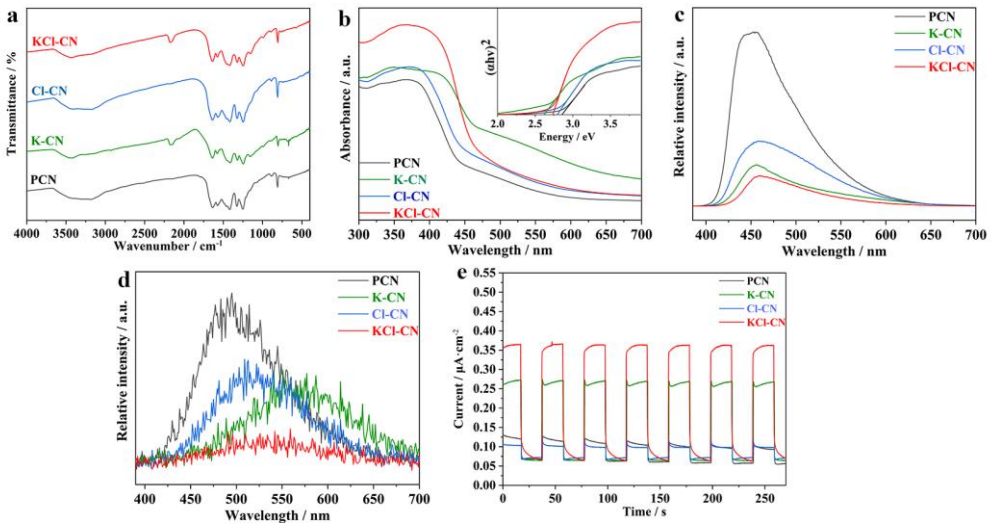

Figure S11. Comparison of polymeric carbon nitride with individual or co-elemental doping. (a) FT-IR spectra, (b) UV-vis spectra (Inset: corresponding Tauc plots), (c) Photoluminescence spectra, (d) Phosphorescence spectra and (e) Periodic on/off photocurrent response curves of PCN, K-CN, Cl-CN and KCl-CN. The periodic on/off photocurrent response plots were recorded under ambient conditions and irradiated by a xenon lamp (Au-Light CEL-HXF300) equipped with a 400 nm cut-off filter at a 0.4 V bias voltage.

As shown in **Figure S11a**, the Fourier infrared characterization of PCN, K-CN, Cl-CN and KCl-CN reveal that all materials retain essentially tri-s-triazine ring units. The ultraviolet-visible (UV-vis) spectra and the corresponding Tauc plots are shown in **Figure S11b**. In comparison to PCN, doped-PCN reduces the band gap and enhances the absorption capacity of visible light. As depicted in **Figure S11c**, the photoluminescence intensity of KCl-CN is lower than that of K-CN, Cl-CN and PCN, indicating a relatively low recombination rate of electrons and holes under light irradiation in KCl-CN.[4] In addition, Phosphorescence spectra (**Figure S11d**) reveal KCl-CN has the lowest phosphor intensity, compared with other samples, indicating that KCl-CN produces the least number of long-lived photoinduced species.[5] Furthermore, the periodic on/off photocurrent response (**Figure S11e**) indicates that KCl-CN exhibits a higher response than K-CN and Cl-CN when illuminated with a light source filtered at 400 nm, suggesting that KCl-CN has the higher carrier concentration among the samples. All the results indicate efficient exciton dissociation in K^+ and Cl^- co-doped polymeric carbon nitride.

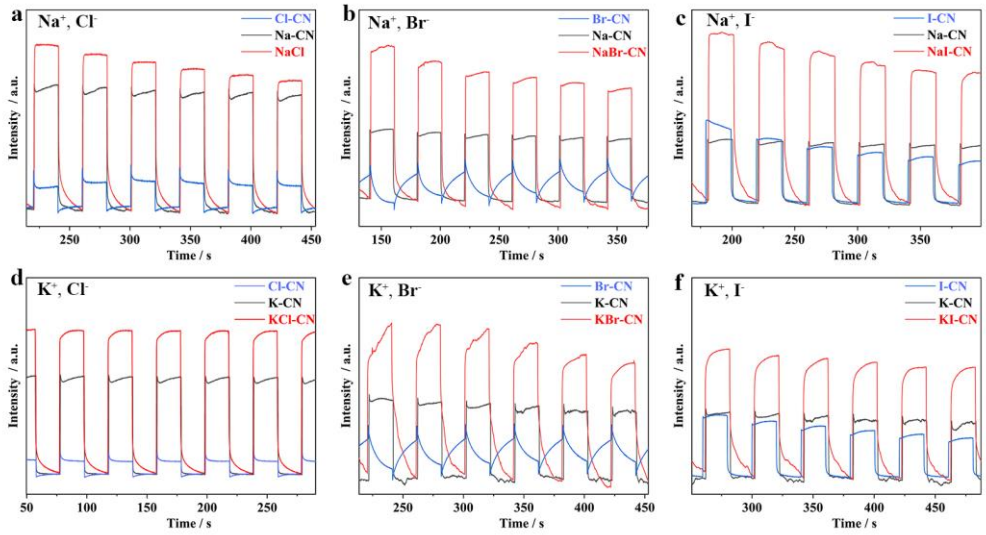

Figure S12. Periodic on/off photocurrent response curves of different anions and cations co-doped polymeric carbon nitride, and their corresponding individual ion doped samples of with cations of (Na^+, K^+) and anions of (Cl^-, Br^-, I^-). The periodic on/off photocurrent response plots were recorded under ambient conditions and irradiated by a xenon lamp (Au-Light CEL-HXF300) equipped with a 400 nm cut-off filter at a 0.4 V bias voltage. To have a better comparison, the photocurrent response for Na/K-CN and Cl/Br/I-CN in the above figures are the same data.

Table S1. The radiative decay results of PCN and KCl-CN.

Sample	τ_1 / ns	τ_2 / ns	τ_3 / ns	Ave.τ / ns
PCN	2.97 ± 0.17	12.15 ± 0.39	0.69 ± 0.02	1.96 ± 0.42
	50.96%	27.23%	21.81%	
KCl-CN	0.87 ± 0.06	3.98 ± 0.16	0.17 ± 7.69	0.49 ± 0.17
	43.72%	22.91%	33.37%	

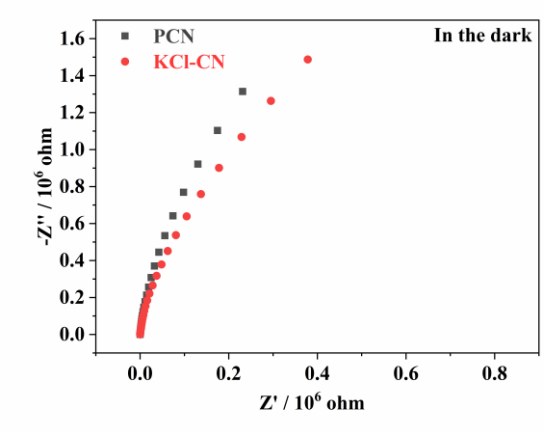

Figure S13. EIS Nyquist plots for PCN and KCl-CN under dark conditions. Electrochemical impedance spectroscopy (EIS) was performed over a frequency range of 0.01 Hz to 10^6 Hz with an AC voltage amplitude of 5 mV.

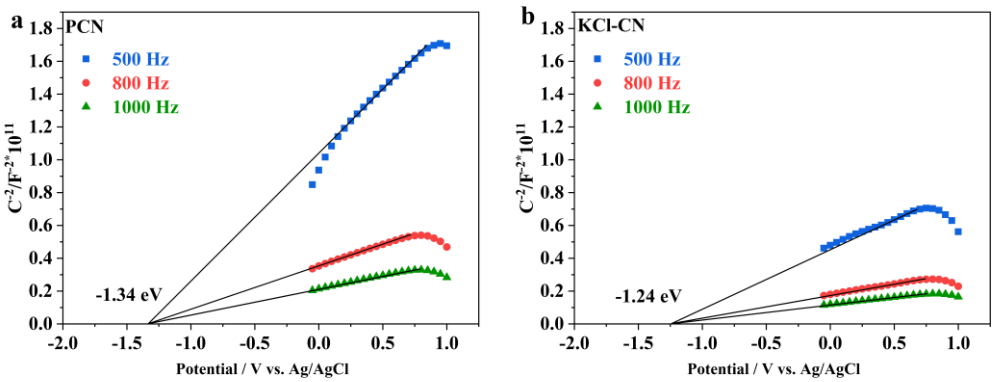

Figure S14. Mott–Schottky plots at 500, 800 and 1000 Hz of (a) PCN and (b) KCl-CN. Mott-Schottky tests was performed with the potentials ranged from -1V to 1V (vs. Ag/AgCl) at the selected frequencies of 500, 800 and 1000 Hz.

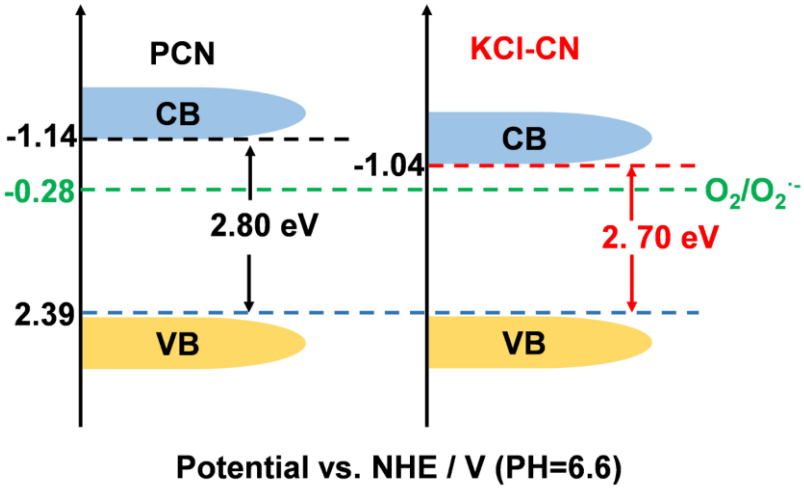

Figure S15. Schematic illustration for band structure of PCN and KCl-CN.

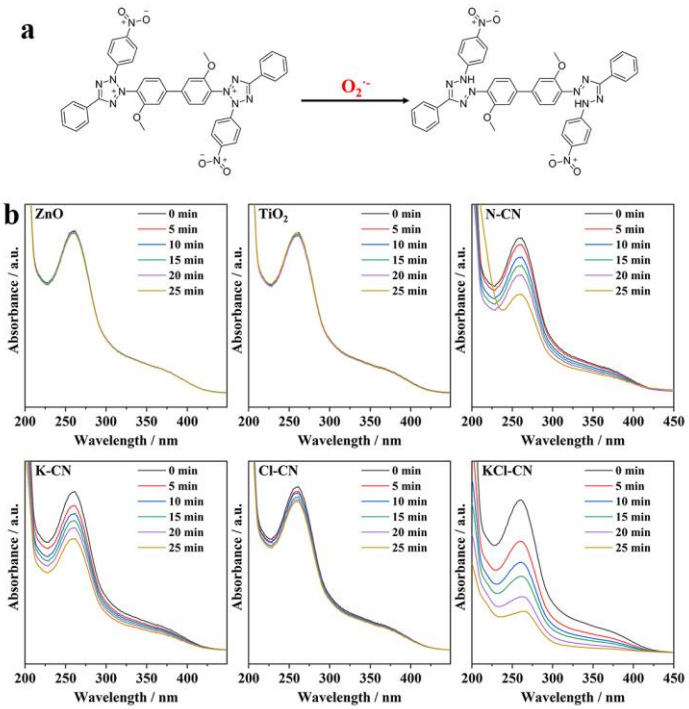

Figure S16. (a) The diagram of NBT degradation by specifically reacting with superoxide radicals; (b) Evolutions of the UV−vis absorption spectra of NBT solution in the different samples under visible light. According to the results, KCl-CN demonstrates a superior ability to generate superoxide radicals compared to the other samples under the same reaction conditions, indicating its highly efficient capacity for superoxide radicals generation.

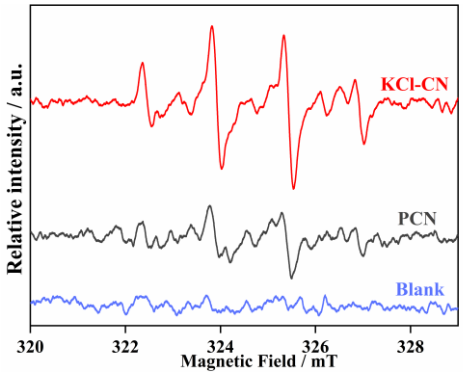

Figure S17. ESR trapping spectra of PCN and KCl-CN in the presence of DMPO in water.

In this study, we also used measurements for electron spin resonance trapping (ESR) to monitor the signal of hydroxyl radical in different samples, and the hydroxyl radical test was carried out in water.[6-8] As depicted in **Figure S17**, KCl-CN has a stronger hydroxyl radical signal than PCN.

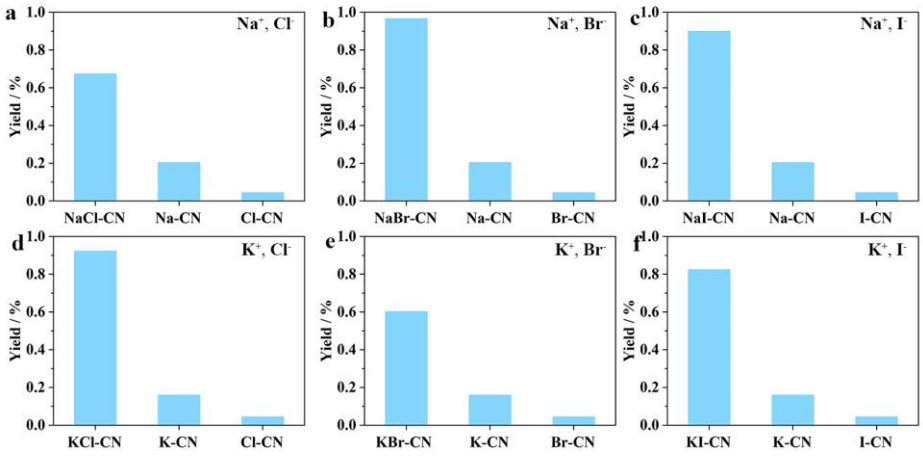

Figure S18. Phenylboric acid oxidation spectrum of different anions and cations co-doped polymeric carbon nitride, and their corresponding individual ion doped samples of with cations of (Na^+, K^+) and anions of (Cl^-, Br^-, I^-). For better comparison, the data for Na/K-CN and Cl/Br/I-CN in the above figures are the same data.

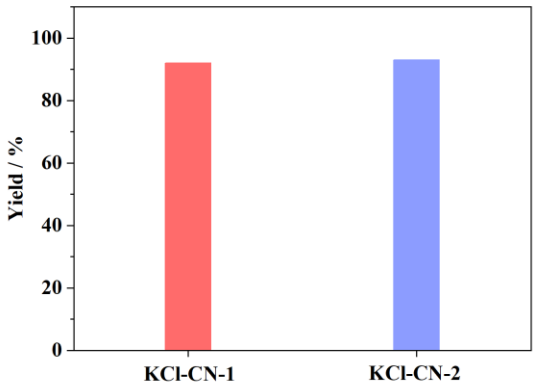

Figure S19. Phenylboric acid oxidation spectrum of different synthesis methods of KCl-CN. The KCl-CN-1, and KCl-CN-2 were synthesized by using potassium chloride or potassium bicarbonate and ammonium chloride as sources of potassium and chlorine, respectively. It is observed that the KCl-CN synthesized by the different methods possess similar catalytic performance.

Table S2. Oxidation of phenylboric acid derivatives by PCN.

Entry	R	Time / h	PCN Yeild / %
1	H	4	6.61
2	p-F	8	trace
3	p-Cl	8	trace
4	p-Br	8	trace
5	p-Me	12	trace
6	m-Me	12	trace
7	o-Me	12	trace
8	p-CHO	12	trace
9	p-CN	12	trace

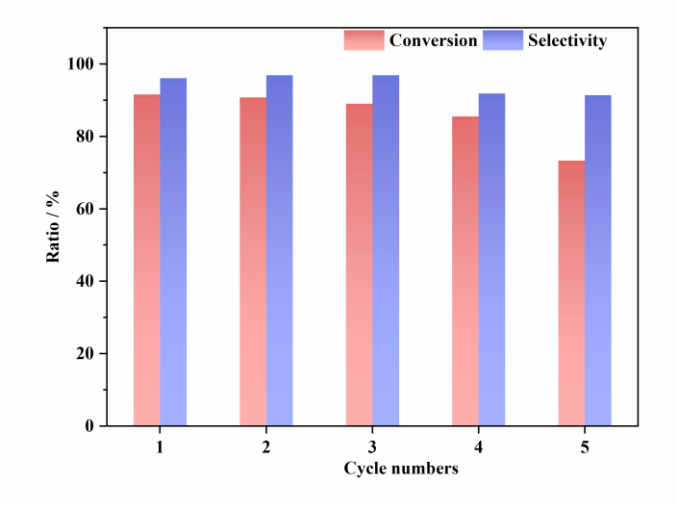

Figure S20. Cycling tests for phenylboric acid oxidation of KCl-CN.

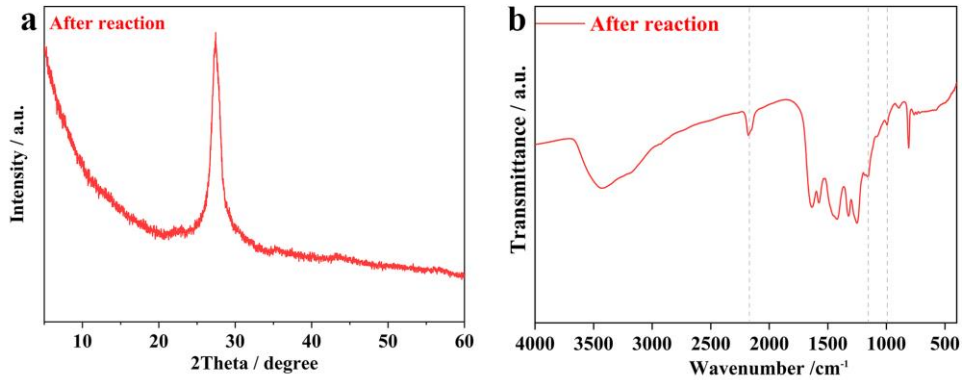

Figure S21. (a) Powder XRD patterns and (b) FT-IR spectra of KCl-CN after cycling tests.

REFERENCES

1. Y. Chen, F. Su, H. Xie, R. Wang, C. Ding, J. Huang, Y. Xu, and L. Ye, *Chem. Eng. J.*, 2021, **404**, 126498.
2. G. Zhang, M. Liu, T. Heil, S. Zafeiratos, A. Savateev, M. Antonietti and X. Wang, *Angew. Chem., Int. Ed.*, 2019, **58**, 14950-14954.
3. G. P. Mane, S. N. Talapaneni, K. S. Lakhi, H. Ilbeygi, U. Ravon, K. Al-Bahily, T. Mori, D.-H. Park and A. Vinu, *Chem., Int. Ed.*, 2017, **56**, 8481-8485.
4. P. Zhang, Z. Wang, L. Li, Z. Li, J. Zhao, H. Wang, X. Zhang and Y. Xie, J. *Phys. Chem. Lett.*, 2023, **14**, 9159-9166.
5. G. Zhang, G. M. Palmer, M. W. Dewhirst, and C. L. Fraser, *Nat. Mater.*, 2009, **8**, 747-751.
6. H. Wang, S. Jiang, W. Shao, X. Zhang, S. Chen, X. Sun, Q. Zhang, Y. Luo and Y. Xie, *J. Am. Chem. Soc.*, 2018, **140**, 3474-3480.
7. K. Dong, Y. Wang, L. Zhang, X. Fan, Z. Li, D. Zhao, L. Yue, S. Sun, Y. Luo, Q. Liu, A. A. Alshehri, Q. Li, D. Ma and X. Sun, *Green Chem.*, 2022, **24**, 8264-8269.
8. G. Grando, G. Sportelli, G. Filippini, M. Melchionna and P. Fornasiero, *Nano Trends*, 2023, **4**, 100028.